Electronic Supplementary Material (ESI) for RSC Advances.

Modeling the Path to > 30% Power Conversion Efficiency in Perovskite Solar Cells with Plasmonic Nanoparticles

Md. Mashrafi, M. Hussayeen Khan Anik, Mst. Farhana Israt, Ahsan Habib, and Sharnali Islam

Supplementary Text ST1: Validation and Benchmarking of Electromagnetic Simulation Methodology

The unique and appealing properties of nanoparticles (NPs) have led to their widespread practical application, setting them apart from bulk materials [1][2]. By manipulating the composition, size, shape, and structure of nanostructures, their characteristics can be tailored to specific requirements [3]. To ensure the accuracy of our model's implementation, it is crucial to calibrate it against experimental observations [4].

In a study by McFarland et al., an optical sensor utilizing a single silver nanoparticle was developed to achieve zeptomole sensitivity [4]. The authors synthesized Ag nanoparticles by reducing silver nitrate with a sodium citrate aqueous solution. While the majority of nanoparticles exhibited a spherical shape with an average diameter of 35 nm, variations in shape, such as prisms, platelets, disks, and rods, were also observed. These silver nanoparticles were exposed to different solvent environments, including nitrogen, methanol, 1-propanol, chloroform, and benzene. Notably, chloroform, with a refractive index of 1.45, was used as the solvent of interest.

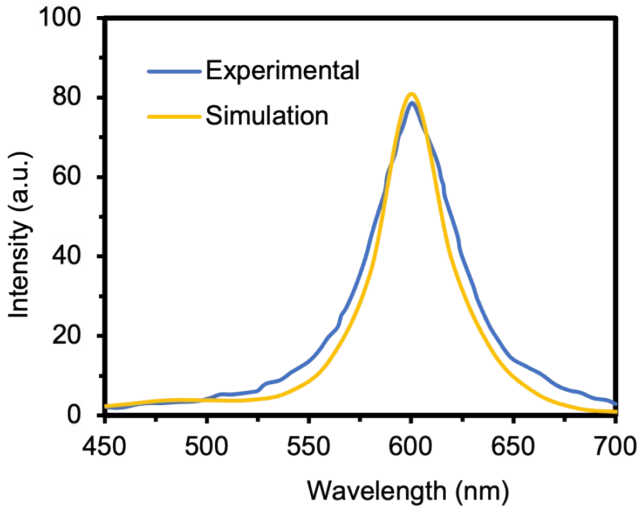

Figure S1: Comparison of our simulated data with existing experimental article [4] for Ag nanomaterial in chloroform solvent. The plot shows the simulated optical intensity obtained from our 3D FEM-based classical electromagnetic simulations in COMSOL, compared with the experimental data. The agreement between our simulated results and the experimental observations confirms the reliability and accuracy of our computational model.

In our study, we aim to validate our computational model by simulating the optical response of a 35 nm spherical silver nanoparticle exposed to chloroform solvent using a three-dimensional finite element method (FEM) electromagnetic simulation in COMSOL. The simulated optical intensity was calculated over the wavelength range of 450 nm to 700 nm, incorporating a wavelength-dependent refractive index. Remarkably, our calculated intensity, as shown in Fig S1, exhibits excellent agreement with experimental findings, providing strong validation for our classical electromagnetic simulations. The resonant peak of the nanoparticle's scattering spectrum, indicative of localized surface plasmon resonance (LSPR), aligns with the experimental observations.

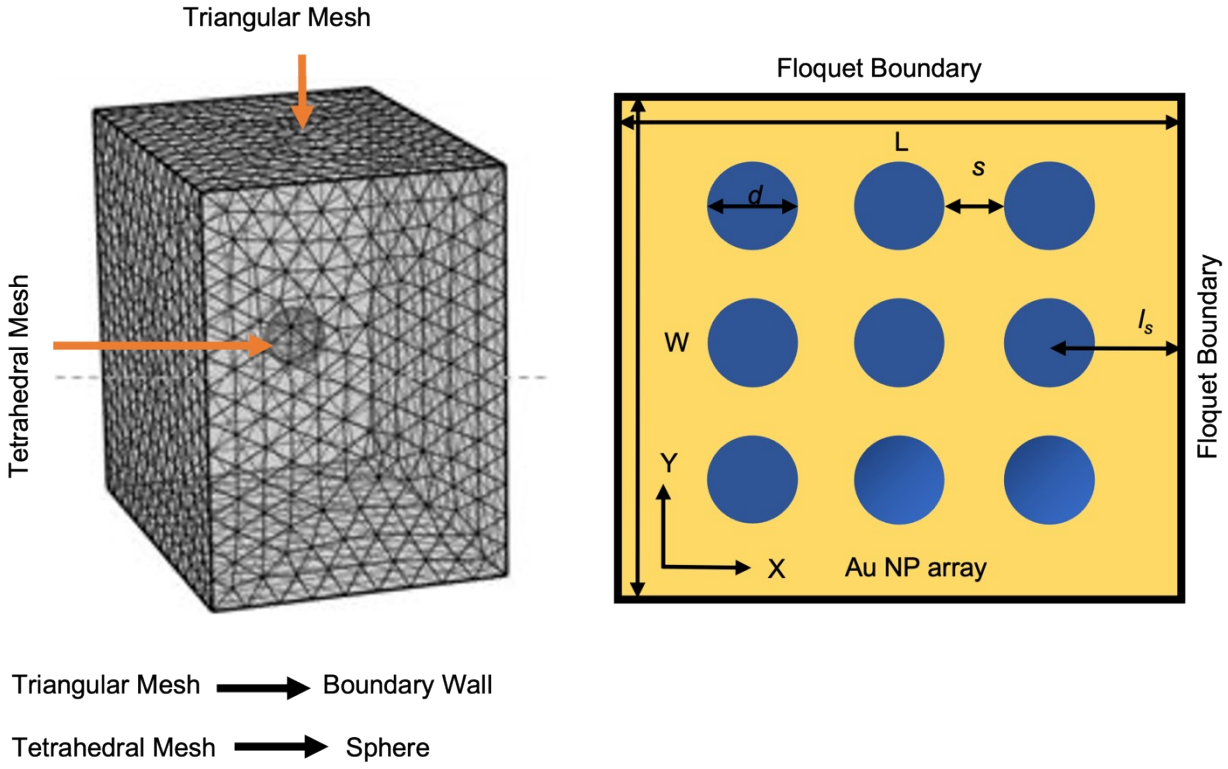

Figure S2: Schematic representation of the model. (a) The physics-controlled meshing of the COMSOL model for calibrating with the experimental work. The smallest mesh is 5.5 nm and the largest one is 44 nm. (b) Top view of the unit cell used in the simulation.

Boundary Condition and Meshing

The mesh for our simulation was created with different element sizes, which are detailed in Supplementary Table 1. In COMSOL, the geometry was divided into small shapes using the mesh node, and a physics-controlled mesh expansion technique was applied, as shown in Figure S2(a). The smallest element size used in our model was 5.5 nm, while the largest was 44 nm. Figure S2(b) provides a top view of the unit cell, which was simulated using Floquet boundary conditions. The model dimensions were represented by L for length, W for width, and d for the diameter of the Ag

nanoparticle. To create a suitable environment, the silver nanoparticle was placed at the center surrounded by chloroform solvent. Floquet periodicity with periodic boundary conditions was employed for the side walls, utilizing ordinary differential equations to solve the frequency domain problem. Floquet periodicity is a suitable method for dealing with spatially periodic geometries [5].

Table S1: Element sizes used in the mesh for the simulation.The table provides information on the element sizes used in the mesh for our simulation. The mesh was created using COMSOL, and different element sizes were assigned to discretize the geometry. The smallest element size used was 5.5 nm, while the largest element size was 44 nm. These element sizes ensured an accurate representation of the geometry and allowed for precise calculations in the simulation.

Maximum element size	44 nm
Minimum element size	5.5 nm
Maximum element growth rate	1.45
Curvature factor	0.5
Resolution of narrow regions	0.6

Supplementary Text ST2: Nano-particle array size optimization

In this work, we have focused mainly on the proof of concept of implanting nanoparticles for increasing the light trapping at the IR region. To illustrate the feasibility and possible advantages of implanting nanospheres into the perovskite layer, we chose a 3×3 array size. We have optimized the size of arrays to investigate the impact on the possible benefits of incorporating nanospheres, which is illustrated in Fig. S3 and Fig. S4. We have found that the absorption doesn't increase significantly after a 3×3 array, which justifies our selection of array size. Considering the computational resources and complexity of the simulations, we opted for this manageable size of the array, which is sufficient to provide meaningful insights into light absorption enhancement.

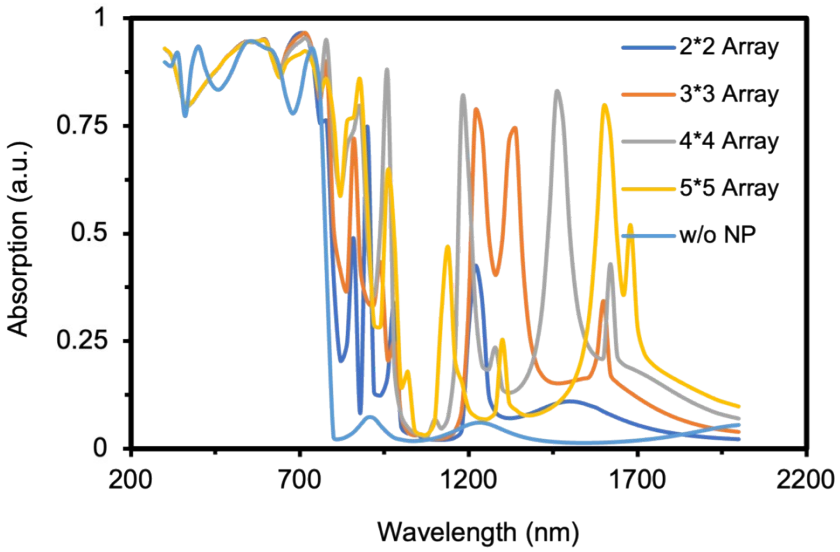

Figure S3: Effect of the number of array variations of nanosphere array in the absorption spectrum wavelength of 300 nm to 2000 nm.

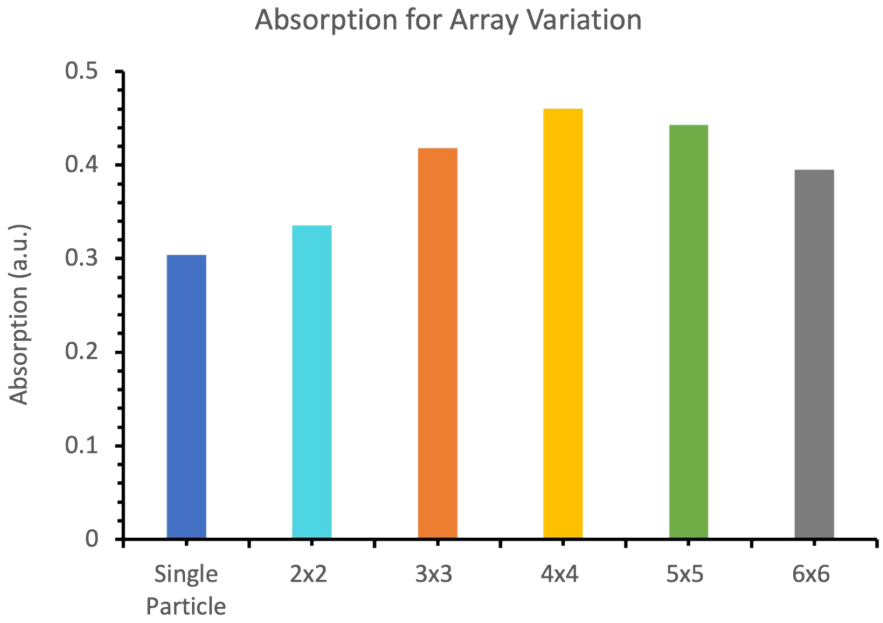

Figure S4: Average absorption of array variation of nanosphere in the absorption spectrum wavelength of 300nm to 2000nm.

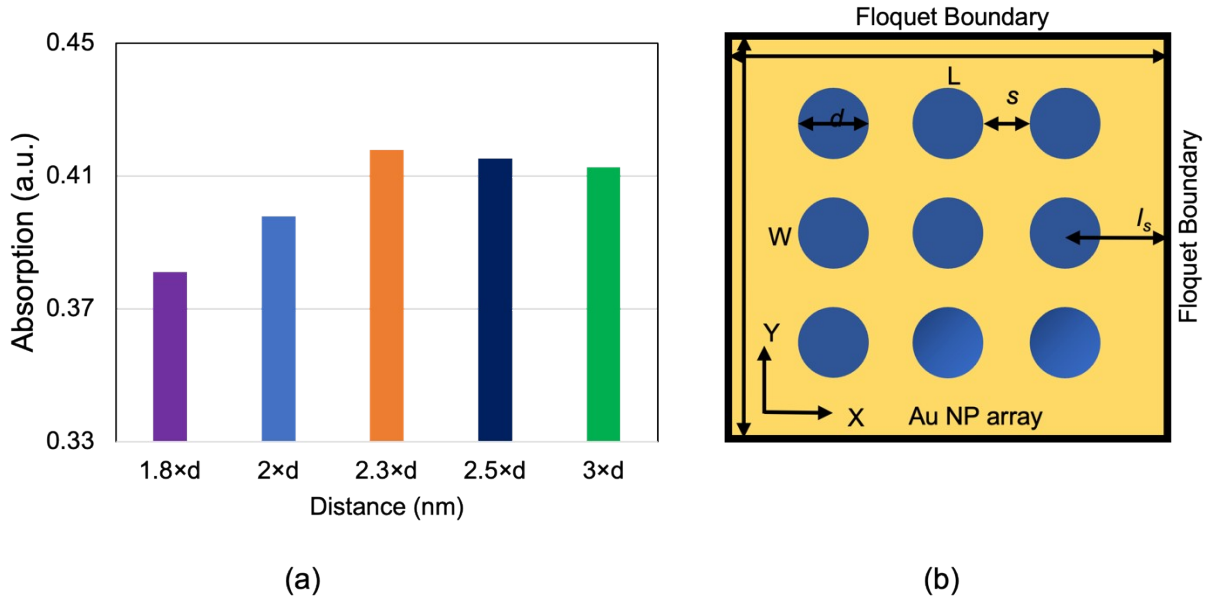

Figure S5: (a) Average absorption for variation of l_s nanosphere in the absorption spectrum wavelength of 300 nm to 2000 nm, having maximum average absorption of 0.4179 for the distance of 2.3×*d*. (b) Top view of the unit cell of array embedded perovskite solar cell; simulated with floquet boundary conditions.

In addition, we have also explored the optimum separation between the center of the nanosphere and the sidewall in Fig. S5(a). The separation between the sidewall and the center of the nearest particle l_s has been calculated as a multiple of *d*, where *d* is the diameter of the nanoparticle and *s* is the distance between the two closest particles shown in Fig S5(b). We have obtained maximum and minimum average absorption of 0.4179 and 0.3812 at the separation of 1.8×*d*, 2.3×*d*, respectively. After the separation distance of 2.3×*d*, the effect of the separation is insignificant, and in our simulation, we used this value to form the unit cell.

Supplementary Text ST3: Validation of the SCAPS model

In our study, we investigate the impact of incorporating plasmonic nanoparticles on the performance of perovskite solar cells (PSCs) using an optical-electrically linked simulation approach. We employ FEM-based COMSOL software to solve the Maxwell equations and determine how the cell's absorption profile affects the rate of exciton formation. The resulting absorption profile is seamlessly loaded into the Solar Cell Capacitance Simulator (SCAPS-1D) software, allowing us to simulate the electrical response of the cell. The accompanying flowchart, depicted in Fig. S6, provides a quick explanation of the optical-electrical coupling method used in our simulations. When we introduce an array of gold nanoparticles (Au NPs) into the absorber layer, the absorption curve generated in COMSOL exhibits a distinct pattern. We subsequently input the modified absorption data into SCAPS-1D for further analysis. This approach, which combines optical and electrical modeling using separate software packages, is widely accepted and supported by several studies [6][7][8].

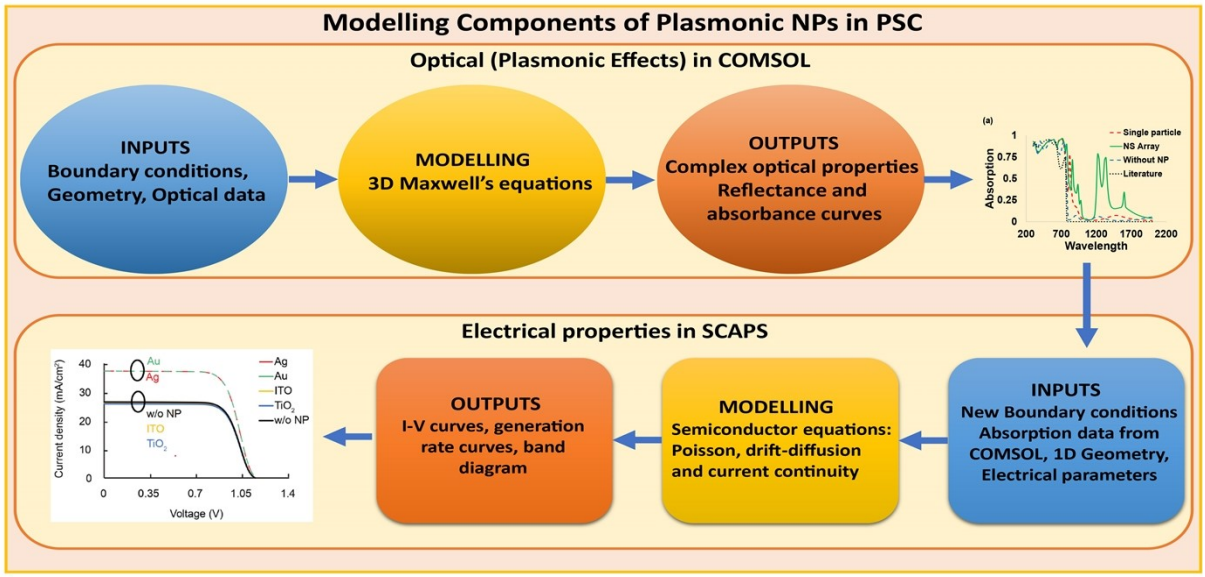

Fig. S6 Coupled optical and electrical modelling components for plasmonic solar cells, complete with the relevant input parameters, models, and output parameters that are necessary for device simulation using COMSOL and SCAPS-1D.

Additionally, another review report corroborates the close agreement between FDTD- and FEM-based optical absorption data, both of which provide good correlations with experimental observations [9].

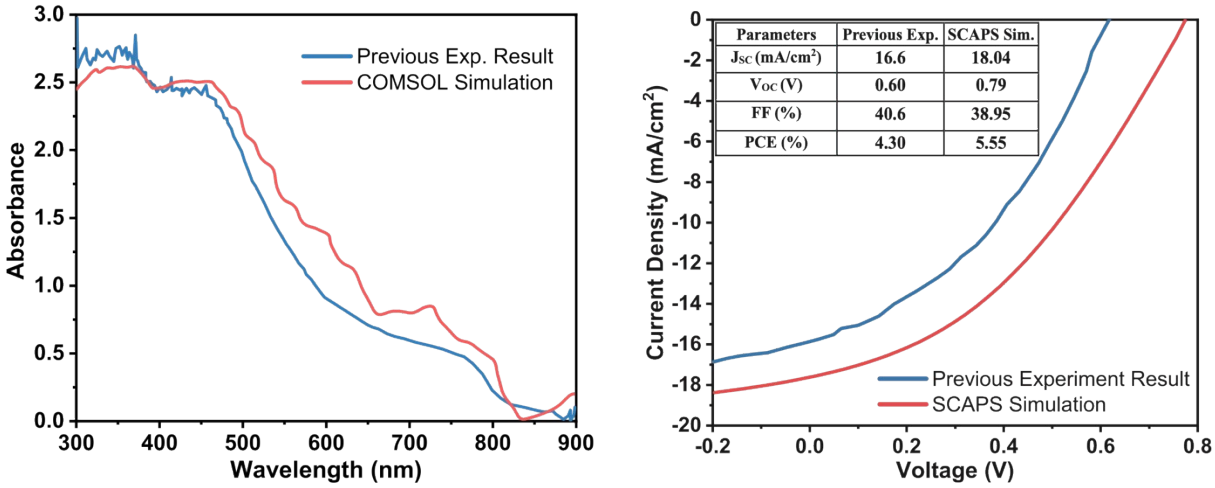

Fig. S7 Comparison between simulations of this work with [10] (a) UV-spectroscopic curve and COMSOL extracted absorption curve. The simulated curve shows a little higher absorption, especially from 500 nm to 800 nm. (b) I-V curves between experimental and SCAPS-generated data. PCE and V_{OC} values are slightly higher for SCAPS simulation as absorption is found to be higher from 500 nm to 800 nm range.

To validate the accuracy of our COMSOL and SCAPS-1D simulations, our next objective is to reproduce the experimental observations for absorption and IV curves. For this purpose, we refer to a previously published experimental and simulation-based study that investigated methylammonium-free perovskite solar devices based on the formamidinium organic cation [10]. This study provided UV-visible spectroscopic absorption curves, SCAPS-generated I-V characteristics, and experimental I-V curves for various absorber layers. We incorporate the thickness, refractive index, and other optical data from this study into our COMSOL model to obtain the absorption curve. In Figure S7(a), a strong correlation between the UV-spectroscopic curve and the COMSOL-extracted absorption curve is observed. However, the simulation predicts slightly higher absorption, particularly in the 500-800 nm range. This disparity can be attributed to the influence of various factors in actual spectroscopic measurements that may affect absorption. In our COMSOL modeling, we assume optimal conditions for variables such as moisture content, temperature, and the vector network analyzer used to estimate the absorption curve. This overestimation is further reflected in our SCAPS-based simulation of the I-V curve in Figure S7(b) (inset table). The fill factor and JSC values agree well with the experimental data, while the SCAPS-generated VOC and PCE are slightly higher than the experimental findings. This discrepancy is reasonable considering the somewhat higher absorption we predicted between 500 nm and 800 nm compared to the experimental results. During the SCAPS simulation, we set the surrounding temperature of the PSC to 330K and carefully accounted for important parameters such as the recombination coefficient, interfacial defects, and capture cross-section of holes and electrons in each layer. These parameters are often overlooked in simulations but are crucial for capturing the experimental conditions [10].The electrical parameters of each layer of PSC used in SCAPS are in the following table (Table S2).

Table S2: Input electrical parameters used in SCAPS-1D for different layers of PSC

Parameters	P3HT (HTL)	TiO_2 (ETL)	$MAPbI_3$	ITO
References	[11]	[12]	[13]	[14]
Thickness (nm)	40	10	400	40
Bandgap (eV)	1.7	3.2	1.5	3.6
Electron Affinity (eV)	3.5	3.9	3.93	4.5
Permittivity	3	9	10	8.9
Effective Density of Stated at CB (cm^{-3})	2×10^{21}	2.2×10^{18}	2.75×10^{18}	2.2×10^{18}
Effective Density of Stated at VB (cm^{-3})	2×10^{21}	1.8×10^{19}	3.9×10^{18}	1.8×10^{19}
Electron Mobility (cm^{-2}/Vs)	1.8×10^{-3}	20	1.0	10
Hole Mobility (cm^{-2}/Vs)	1.8×10^{-2}	10	1.0	10
Donor Doping Density, N_D (cm^{-3})	1×10^{13}	1×10^{16}	1×10^{9}	1×10^{15}
Acceptor Doping Density, N_A (cm^{-3})	-	-	1×10^{9}	-
Defect Density, N_t (cm^{-3})	1×10^{14}	1×10^{14}	1×10^{14}	1×10^{12}
Electron Thermal Velocity (cm/s)	1×10^{7}	1×10^{7}	1×10^{7}	1×10^{7}
Hole Thermal Velocity (cm/s)	1×10^{7}	1×10^{7}	1×10^{7}	1×10^{7}

Capture Cross Section Electron (cm^2)	1×10^{-14}	1×10^{-14}	1×10^{-15}	1×10^{-16}
Capture Cros Section Holes (cm^2)	1×10^{-14}	1×10^{-14}	1×10^{-15}	1×10^{-16}
Radiative recombination coeff. (cm^3/s)	-	-	1×10^{-9}	-

References:

[1] M. C. Daniel and D. Astruc, "Gold Nanoparticles: Assembly, Supramolecular Chemistry, Quantum-Size-Related Properties, and Applications Toward Biology, Catalysis, and Nanotechnology," *Chem. Rev.*, vol. 104, no. 1, pp. 293–346, 2004, doi: 10.1021/cr030698+.

[2] H. Kato, "In vitro assays: Tracking nanoparticles inside cells," *Nat. Nanotechnol.*, vol. 6, no. 3, pp. 139–140, 2011, doi: 10.1038/nnano.2011.25.

[3] S. E. Skrabalak *et al.*, "Nanocages," *Catal. from A to Z*, vol. 41, no. 12, pp. 1587–1595, 2020, doi: 10.1002/9783527809080.cataz11280.

[4] A. D. McFarland and R. P. Van Duyne, "Single silver nanoparticles as real-time optical sensors with zeptomole sensitivity," *Nano Lett.*, vol. 3, no. 8, pp. 1057–1062, 2003, doi: 10.1021/nl034372s.

[5] Y. Zhang, N. Feng, L. Wang, Z. Guan, and Q. H. Liu, "An FDTD Method for Fully Anisotropic Periodic Structures Impinged by Obliquely Incident Plane Waves," *IEEE Trans. Antennas Propag.*, vol. 68, no. 1, pp. 366–376, 2020, doi: 10.1109/TAP.2019.2935140.

[6] M. K. Omrani, R. Keshavarzi, M. Abdi-Jalebi, and P. Gao, "Impacts of plasmonic nanoparticles incorporation and interface energy alignment for highly efficient carbon-based perovskite solar cells," *Sci. Rep.*, vol. 12, no. 1, pp. 1–10, 2022, doi: 10.1038/s41598-022-09284-9.

[7] M. Farhat, S. Kais, and F. H. Alharbi, "Plasmonically Enhanced Schottky Photovoltaic Devices," *Sci. Rep.*, vol. 7, no. 1, pp. 1–9, 2017, doi: 10.1038/s41598-017-14528-0.

[8] S. S. Nishat *et al.*, "Performance Analysis of Perovskite Solar Cells Using DFT-Extracted Parameters of Metal-Doped TiO2Electron Transport Layer," *J. Phys. Chem. C*, vol. 125, no. 24, pp. 13158–13166, 2021, doi: 10.1021/acs.jpcc.1c02302.

[9] A. Ali, F. El-Mellouhi, A. Mitra, and B. Aïssa, "Research Progress of Plasmonic Nanostructure-Enhanced Photovoltaic Solar Cells," *Nanomaterials*, vol. 12, no. 5, p. 788, 2022, doi: 10.3390/nano12050788.

[10] S. Karthick, S. Velumani, and J. Bouclé, "Experimental and SCAPS simulated formamidinium perovskite solar cells: A comparison of device performance," *Sol. Energy*, vol. 205, no. March, pp. 349–357, 2020, doi: 10.1016/j.solener.2020.05.041.

[11] M. K. Hossain, M. Humaun, K. Rubel, G. F. I. Toki, and I. Alam, *Effect of various electron and hole transport layers on the performance of CsPbI 3 -based perovskite solar cells : A numerical*

investigation in DFT , SCAPS-1D , and wxAMPS frameworks. .

[12] N. Mashhadi Seyyed Abadi, M. Banihashemi, and A. Kashani Nia, “Effects of HTL/ETL properties on the performance of (FAPbI3)0.85(MAPbBr3)0.15perovskite solar cells,” *J. Phys. D. Appl. Phys.*, vol. 54, no. 33, p. 334001, 2021, doi: 10.1088/1361-6463/ac036f.

[13] M. S. Jamal *et al.*, “Effect of defect density and energy level mismatch on the performance of perovskite solar cells by numerical simulation,” *Optik (Stuttg).*, vol. 182, no. December 2018, pp. 1204–1210, 2019, doi: 10.1016/j.ijleo.2018.12.163.

[14] F. Azri, A. Meftah, N. Sengouga, and A. Meftah, “Electron and hole transport layers optimization by numerical simulation of a perovskite solar cell,” *Sol. Energy*, vol. 181, no. December 2018, pp. 372–378, 2019, doi: 10.1016/j.solener.2019.02.017.